

Visual Representations for Semantic Target Driven Navigation

Arsalan Mousavian, Alexander Toshev, Marek Fišer, Jana Košecká, James Davidson

{amousavi, kosecka}@gmu.edu
{toshev, mfisher, jcdavidson}@google.com

Abstract. What is a good visual representation for autonomous agents? We address this question in the context of semantic visual navigation, which is the problem of a robot finding its way through a complex environment to a target object, e.g. *go to the refrigerator*. Instead of acquiring a metric semantic map of an environment and using planning for navigation, our approach learns navigation policies on top of representations that capture spatial layout and semantic contextual cues.

We propose to using high level semantic and contextual features including segmentation and detection masks obtained by off-the-shelf state-of-the-art vision as observations and use deep network to learn the navigation policy. This choice allows using additional data, from orthogonal sources, to better train different parts of the model – the representation extraction is trained on large standard vision datasets while the navigation component leverages large synthetic environments for training. This combination of real and synthetic is possible because equitable feature representations are available in both (e.g., segmentation and detection masks), which alleviates the need for domain adaptation.

Both the representation and the navigation policy can be readily applied to real non-synthetic environments as demonstrated on the Active Vision Dataset [1]. Our approach gets successfully to the target in 54% of the cases in unexplored environments, compared to 46% for non-learning based approach, and 28% for the learning-based baseline.

Keywords: Navigation, Target Driven Navigation, Semantic Understanding

1 Introduction

Visual perception is one of the key capabilities of intelligent robotic agents enabling them to purposefully act in an environment. The question then naturally arises as to what is the most appropriate representation derived from visual observations that can support various robotic tasks? We study this question in the context of target-driven semantic visual navigation, where an agent deployed in an unexplored environment is tasked to navigate to a semantically specified goal, e.g. *go to refrigerator*.

Traditional approaches for this problem focus on 3D metric and semantic mapping of the environment [2,3] followed by path planning and control. Such approaches typically require building a 3D map ahead of time before planning and do not exploit general semantics and contextual cues in the decision making stage. More recently, success of data driven machine learning strategies for variety of control and perception problems opens new avenues for overcoming the limitations of the previous approaches [4,5,6,7,8]. The gist of these methods is to directly learn a mapping between observations and actions for the task at hand.

In this work we propose to use high-level semantic and contextual features included in segmentation and detection masks obtained by the state-of-the-art and learn navigation policy from these observations. The key advantage of this approach is combining learning the navigation strategy, with learning how to use these visual representations. Thus, an agent can leverage extensive navigation experience in similar environments, discover commonly encountered objects and contextual cues and learn policies that can generalize to previously unseen environments.

We demonstrate that the choice of proposed visual representations enables the following:

Better generalization Real data for navigation problems is scarce. Having representations, which enable better generalization of the navigation model on small data is thus desirable.

Transferable representations It takes advantage of amply available simulated environments. Such data has different statistics than the real one, and therefore it cannot be easily used.

Integration of complementary data It leverages orthogonal dataset to learn underlying representations that are meaningful to the set of tasks we are solving. In our case, we want to leverage existing object detection and semantic segmentation trained on standard vision datasets to apply to target driven navigation.

The navigation policy is learned on top of these representations (see Fig. 1). These masks capture the outlines of a wide range of foreground and background objects and stuff, and as such provide a detailed description of the scene. This description is concise and relevant for navigation – target objects, contextual objects, obstacles, etc. Despite its simplicity, such representation addresses the above challenges and leads to strong navigation performance on *real data*, usually not demonstrated by the majority of learning-based navigation approaches. One of the reasons is that it allows use of large quantities of additional synthetic data with highly relevant for navigation labels.

First, the detectors and semantic segmentation are trained using standard vision datasets, which contain strong location labels. Thus, these representations by design are suited for real data.

Second, during training of the navigation component we can mix the real data from the environment with larger synthetic data from simulated environments,

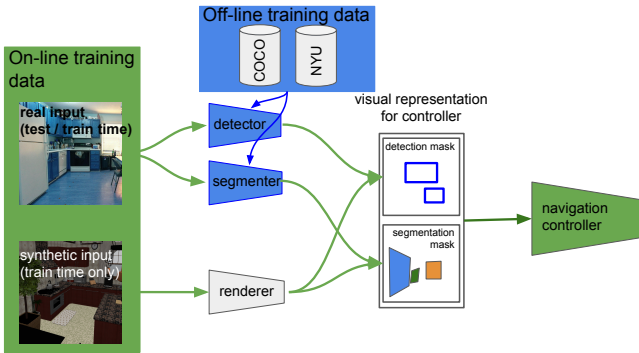


Fig. 1: Segmentation and detection masks as a representation for navigation. It allows for additional on-line data (green) and off-line data (blue). Further, there is no need for domain-adaptation when training on simulated data, as the renderer can provide masks.

which we call on-line data. The synthetic data is substantially more plentiful and has realistic object arrangements. The rendering, however, is usually far from realistic. We can circumvent this by using directly the segmentation and detection masks associated with the data instead of rendering pixels. Thus, the chosen representation bridges the reality gap often encountered when using simulated data and removes the need for domain adaptation.

Further advantage of the above representation choice is leveraging off-the-shelf state-of-art detectors and segmenters, without the need to fine-tune them as part of the training. As in many learning based systems actually the feature extractor contains the bulk of the model parameters (e. g. ,see [4]), we can have comparably to such approaches larger number of parameters dedicated to the navigation controller. We perform a thorough investigation of the above representation. We contrast and combine it with raw RGB and depth inputs. Despite it being inherently lossy, the ability to leverage large strong vision networks and additional data leads to superior results compared to training a more general representation together with the navigation component.

Given the proposed representation, a further contribution of this work is the choice of the model and training of the navigation policy. As we have a map of the environment at train time represented as a graph, we can use an optimal path planning algorithm as form of stronger supervision to estimate the progress toward the goal after taking an action. The controller learns to predict this progress value and uses it to pick an action at test time. We investigate several models – a feed-forward memory free model as well as model with internal state implemented using an LSTM [9]. We use both synthetic [10] and real environments [1] to train and evaluate the learned navigation policy with detailed ablation study of the choice of visual representations and model architecture. This proposed model reaches the target successfully 54% of times on novel previously unseen environments.

2 Related work

The proposed work is related to different approaches towards visual navigation. Classical techniques for navigation typically start with map construction, followed by planning and execution of the planned trajectories. The mapping stage uses visual observations for simultaneous localization and construction of semantic and metric or topological map (see for an extensive review [2,3] of SLAM). Given the model of the environment the state-of-the art planning and control strategies can be found in [11]. More recent methods bypass the mapping and explicit pose estimation steps and learn the navigation strategies directly. The existing learning based approaches differ in the architectures, size and the complexity of the models, the cost of the training stage, generalization capability and the type of supervision. The existing formulations consider either *point-to-point* navigation strategy, where the goal is given as coordinate in the ego-centric coordinate frame [12] or *target-driven* navigation strategy, where the image of the target is given as an input [7]. The later approach follows the success of A3C reinforcement learning (RL) that in visually simpler game environments [13] exceeded human performance. Synthetic CG environments of indoors household scenes and targets were considered in [7]. This target-driven approach proposes feed-forward architecture, which takes as an input an image of the initial state, the target state and uses a Siamese architecture to train scene specific (kitchen, dining room, living room) reinforcement learning policies using modified A3C algorithm. The common embedding is learned between target and current observation. The approach affords generalization to previously unseen targets in the previously seen rooms is experimentally evaluated. Additional RL learning strategies and associated deep learning architectures are discussed in [14] and references therein. The experiments were carried out in synthetic 3D maze environments with a single goal. The observations in these environments are simplistic mazes and do not exhibit the complexity of real world settings. Authors in [14] suggested to overcome the difficulties associated with sparse rewards suggesting various auxiliary losses for depth prediction and loop closure detection. For simulated indoors environments basic RL strategies (feed-forward A3C, A3C with LSTM and Direct future prediction method of [15]) for point goal and room goal prediction were benchmarked in Minos environment [16].

Work of [12] proposes an approach where mapping and planning are considered jointly and are put together into a unified architecture that can be trained to leverage regularities of indoors environments. Mapper produces local ego-centric belief in the top-down view and planner uses this belief to plan paths to specific goals. The learning follow supervised imitation learning paradigm along with hierarchical Value Iteration Networks (VIN) in place of planning component. The whole architecture is trained jointly using observations from 3D reconstructions of real-world environments as provided by Matterport3D [17] dataset.

The broader area of active and embodied perception received increased interest in computer vision community focusing both on navigation, task planning and visual question answering tasks yielding different simulation environments derived from SUNCG [10] or Matterport3D [18,16] datasets. While there are

numerous architectures for visual question answering task [19,20,8], with the exception of [8] the evaluation metrics do not explicitly consider navigation component.

On the control for navigation side, traditional imitation learning methods which use Deep CNN for end-to-end learning of the control tasks are typically state-less. Simple option to for adding some state to the network is to use some history of observations and actions as an input. Since this alternative is not scalable, the natural option is to consider a network that has an internal state such as recurrent neural network or is recent augmentations which use external memory with read and write operators can be learned as part of the training process [21]

3 Navigation Model

3.1 Setup

We address the problem of navigating to a target, defined by its class label, by using purely visual observations. This problem can be represented as a partially observable Markov decision process (POMDP) (S, A, O, P, R_c) . The state space S consists of the pose of an agent, which is not observable. The action space A is a discrete set of turns and translations of pre-defined lengths inducing a lattice structure—described in detail in experiments sections. Observation space O are raw RGB and depth images. The probability $P(s'|s, a)$ reflects the transition to a new state s' after an execution of an action a in the current state s . Finally, the reward R_c expresses how far away is the agent from the target c and can be defined as the negative of the shortest path between the current state $s \in S$ and the target c : $R_c = -d(s, c)$.

Within the above setup, our navigation policy is represented by a Neural Network $\pi(a|o; c)$ which given the target class label c and an observation $o \in O$ predicts an action $a \in A$. The policy is to generate a sequence of actions that move the agent from its starting position to the target.

3.2 Visual Representations

The focus of this work are representations one can extract from the visual observations. Such representations, denoted by $f(o) = (\dots, f_i(o), \dots)$, are the bridge between the raw signal and the controller. Thus, the model can be written as $\pi(a|f(o); c)$. In robotic applications the raw observations consists of RGB image, which is often times augmented with a depth image, derived from Radar, LiDAR or stereo. Therefore, a common choice of f is a ConvNet [22,23], which is typically designed for and pre-trained on a large classification dataset [24]. Such a network is used to produce a vectorial embedding of the image.

To this end we consider the following representations:

ObjDet: A set of object detection masks. We use Faster R-CNN [25] object detector trained on COCO [26]. The detector output is converted to a $H \times$

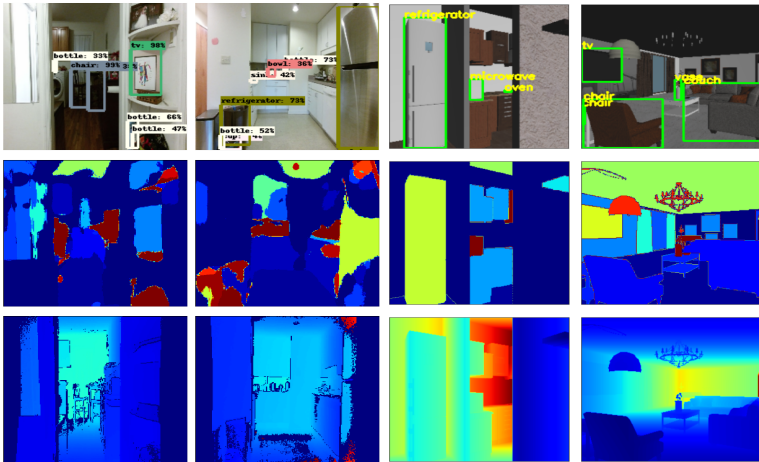


Fig. 2: Visualization of detections (top), segmentations (middle) and depth (bottom). While for real data (left) we use off-the-shelf detector and segmenter, the output on the simulated data (right) comes from the labels in this data and the renderer.

$W \times C_{det}$ mask where H and W are the height and width of the image and C_{det} is the total number of object categories in COCO. The j^{th} channel contains all detected boxes for the j^{th} class as 0/1 masks.

Sseg: The output of the segmenter defined by Mousavian et al. [27] that is trained on NYU V2 dataset [28]. The resulting representation is a $H \times W \times C_{sseg}$ mask stack where C_{sseg} is the number of categories in the NYU V2 dataset.

Depth: The raw depth channel converted to $H \times W \times 2$ where the first channel is the normalized depth values coming from the sensor and the second channel is a binary mask that indicates whether a pixel has a valid or missing depth.

RGB: The penultimate layer output of the ResNet-50 [23] trained on ImageNet.

RGB is the standard feature extractor. It is the most general one, as the output is a real valued vector that in theory can capture all information needed by the task. Since it is trained on a classification dataset, it might not capture all details needed for navigation. Thus, it is often times fine-tuned as part of the controller network. This presents a challenge as *RGB* constitutes a large network.

Further, *RGB* cannot be easily used on both real and simulated data as the network produces different outputs on the different domains. A large body of work focuses on domain adaptation [29,30] and its applications to robotics [31,18]. Such approaches are hard to train as they rely on still relatively unstable generative adversarial network setups.

Both *ObjDet* and *Sseg* address some of the above challenges. They do capture scene layouts, obstacles, location of target objects (see Fig. 2). And as we em-

pirically show later, despite they being lossy compared to *RGB*, they do capture most of the necessary information for navigation without the need of fine-tuning. Thus, large segmentation and detection networks are used without being part of the training of navigation controller, which makes the optimization of the latter easier and more stable.

Another advantage of *ObjDet* and *SSEg* is that there is no need for domain adaptation. While semantic segmentation and detectors are used on real data, in simulation the object masks and bounding boxes can be generated by the renderer (see Fig. 2). Then the gap between real and simulation is related to the quality of the segmentation and detector. This setup is particularly timely as research on object detection [26], semantic segmentation [32] and depth estimation [27] has been propelled by deep learning methods with variety of high performing models available. We show empirically, that by using simulation with this representation we achieve substantial improvement without any domain adaptation.

3.3 Model

The model $\pi(a|f(o); c)$ using the above representation is a Deep Neural Network (see Fig. 3). In addition to the current observation the model takes as an input a description of the target in the form of one-hot vector over a pre-defined set of classes. This secondary input is concatenated with the observation representations and modulates the network behavior.

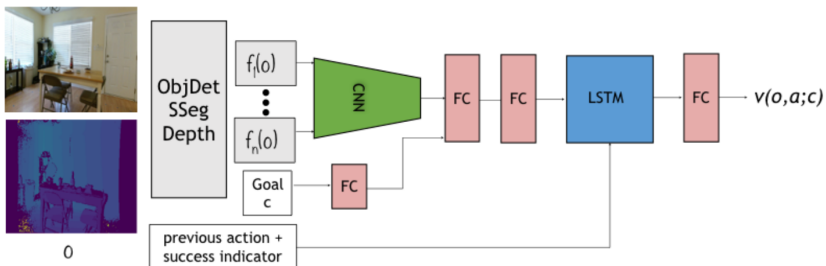


Fig. 3: Model Overview: The observation representation, together with a target description, the previous action and a binary collision indicator is passed to an RNN. The model predicts the cost $v(o, a; c)$ of taking action a at the current state. Finally, the controller takes the action with the lowest cost (see. (3)).

We experiment with several architectures for the policy network. In addition to a simple feed-forward architecture, we use a stateful one in the form of a Long-Short Memory Net (LSTM) [9] to represent an internal state during execution. This choice leads to superior performance to purely feed-forward nets in our experiments. Sec. 4)

The architecture of the network is shown in Fig 3. The CNN architecture that we use for extracting representation from each feature extractor $f_i(o)$ consists of three convolutional layers and a fully connected layer, all using ReLU as activation. The convolution layers have kernel sizes $8 \times 8 \times 8$, $4 \times 4 \times 16$, $3 \times 3 \times 16$ and strides of 4, 2, 1 respectively. The fully connected layer produces 128 dimensional embedding for each modality except *RGB*, for which we use pretrained ResNet50. The input target c is presented with one-hot vector and gets projected to embedding of 128 dimensional. All the embeddings are concatenated with each other and processed with a series of fully connected layer and LSTM. The size of the fully connected layers and LSTM is 2048.

Further, we experiment with explicitly using the history of previous action as an input to the model along with a binary indicator whether it resulted in a collision or not. We assume that there is a collision detection module, which is commonly present in robot systems. This input helps the model choose a different recovery action if a collision is experienced.

3.4 Training

In our navigation setup we have full knowledge of the environment at train time. We consider discrete setting where the environment can be described by a graph G_e with nodes representing a discrete set of states – poses (locations and headings) of the agent. Edges in this graph correspond to possible state transitions. Thus, for the problem of getting to an object one can use shortest path planning algorithm. At test time, however, the environment map (graph) is not known. Nevertheless, we would like to learn a controller which performs as close as possible to an optimal path by exploiting general contextual cues. For this, instead of employing Deep Reinforcement Learning, where at train time the agent is to discover the optimal path guided only by a reward definition, we use strong supervision from a path planning algorithm.

The above setup falls into the domain of imitation learning. Common approaches include behavior cloning [33] and Dagger [34]. In such approaches the agent is trained to emulate an expert, in this case a path planner, producing demonstrations. One drawback of the above approaches in our setup, however, is that often times multiple actions at a given state can follow an optimal path. And when an action is not optimal, it isn't necessarily incorrect. Therefore, we train our agent to predict the cost of an action a , which is defined as the 'progress' toward the goal (an approximation of the negative of the value function in RL) – the reduction of the shortest distance $d(s, c)$ from current state s to the target c after taking a :

$$y(s, a; c) = \sum_{s'} P(s'|s, a) d(s', c) - d(s, c) \quad (1)$$

The value of the above cost reflects the 'correctness' of an action. Details of the transition model, $P(s'|s, a)$, are described in the experimental section. Using the above definition of state-action cost, we train a neural network $v(o, a; c)$ to

predict the above cost directly from observations:

$$Loss = \frac{1}{|C||S||A|} \sum_{c \in C} \sum_{s \in S} \sum_{a \in A} (v(o, a; c) - y(s, a; c))^2 \quad (2)$$

If an action a leads to a collision the corresponding $v(o, a; c)$ will be set to $+2$. The final navigation controller chooses at test time an action with the lowest predicted cost:

$$\pi(a|o; c) = \arg \min_{a \in A} v(o, a; c) \quad (3)$$

Note that although we do not consider history of observations explicitly in the above formulation, it is modeled implicitly by the LSTM component of our model.

Discussion During training we use both real and simulated environments. The real data comes from dense scans of real houses. Both environments are discrete in nature – we work with a pre-defined set of possible locations and orientations; the action space is discrete. Thus, we can enumerate all possible state-action pairs, as shown in the loss in Eq. (2). Contrary to most other POMDP setups, $S \times A$ is not prohibitively large and we are guaranteed to visit all state-action pairs eventually. Thus, there is no need of state exploration guided by a policy.

4 Experiments

We used two datasets for our experiments.

Active Vision dataset [1] consists of dense scans of 16 different houses, some houses scanned multiple times. Each scan is a collection of images captured on a regular grid, for each location in the grid there are 12 images at 30° intervals. The dense scan allows for a realistic traversal of a real environment, where the actions can move the agent from one location to another. We consider a discrete set of actions `{move_forward, move_back, move_left, move_right, stop, rotate_ccw, rotate_cw}`. If there is no next view associated with the action, the action is considered to be a collision. We manually labeled target views for the following five categories: `{dining_table, refrigerator, television, couch, microwave}`. Target view for an instance of these categories is any view that the object is visible in and it is maximum two steps away from the goal.

SUNCG dataset [10] consists of manually designed synthetic models of houses. We use the subset of 200 environments selected by [8]. In order to make the policies transferable, for each house we find a collision-free grid, defined as in AVD. A viewpoint belongs to a target view V_c if at least 4% of the pixels correspond to semantic class c and the distance of the any instance of category c from the viewpoint is less than 1 meter. The semantic categories labels provided by SUNCG dataset are mapped to NYU V2 labels [28]. We also generate detection bounding boxes for the categories of MS-COCO dataset [26] from the ground truth segmentation and instance masks.

Train/Test Splits Evaluation is done on the real images from the AVD. We define two different train/test splits. In both splits, we hold out three scans for the evaluation and the rest of the environments is used for training. The first split, called *similar environments*, has the same environment in both train and test, however different scans. This setup tests how well does our system perform when it has seen the environment during training, albeit not scanned in the same way. The second split, which is called *different environments* split, keeps the environments for testing different from the ones for training. Thus, it is used to evaluate generalization on unseen environments.

4.1 Training Details

Each minibatch consists of losses formulated over 8 random trajectories. Each trajectory is generated by selecting a random environment, from either AVD or SUNCG, generating a random goal and target and selecting the first 20 locations from this trajectory.

The output of all $f_i(o)$ except the raw image is resized to 64×64 pixels. Raw images are resized to 299×299 pixels to match the resolution at which the ResNet50 has been trained on.

We use Adam Optimizer, learning rate of 10^{-4} and exponential decay schedule with decay rate of 0.98 at every 1000 steps. The model is optimized for 200 000 iterations on 40 GPUs, which takes 16 hours.

4.2 Analysis

In the evaluation we study the effect of different choices of visual representations on the final performance, their effect on generalization of the controller training, the effect of using simulated data for training jointly with real images and some choices affecting the model architecture. For the analysis in this section, the policy is unrolled for 100 steps and the evaluation is terminated either when the number of steps exceeds 100 or the agent predicts action `stop`. Initial locations are chosen randomly and they are fixed for all the experiments. The performance of the agent is measured by success rate which is the fraction of runs which end within 5 steps from the goal. The maximum distance from the init points to the goals is 35 steps.

RGB vs Semantic Representation: The first question we address is whether using segmentation and detection outputs can be a sufficient and even better representation than fine-tuning a general ConvNet on the raw observations. We combine *SSeq* and *ObjDet* as explained in Sec. 3.3. For *RGB* and *ObjDet* we use an ImageNet pre-trained ResNet-50, which we further fine-tuned as part of the navigation model training.

The success rate representation combinations across the two evaluation splits are presented in Fig. 4. We compared the success rate of each representation with and without depth. We observe that using pre-trained ResNet-50 results

in superior performance on the *similar environment* split but it has poor generalization for *different environment* split. Since the embedding that is coming from Resnet-50 is significantly larger than the one that is coming from semantic representation (2048 vs 128), it is much easier to overfit in the presence of the limited amount of training data. We also tried adding a bottleneck layer to the Resnet-50 embedding to reduce the embedding size from 2048 to 128 but it did not help improving the success rate. Adding depth maps to ResNet-50 embedding increases the information that is fed to the network which leads to more overfitting on the *similar environment split*. However, when the model trained on *different environment split* *SSeg* and *ObjDet* demonstrate better generalization. In particular both representations outperform raw pixels by 15% and 8%. Thus, the proposed representation are better suited to be used on unexplored environments, which is the common use case as we more often have no access to the deployment environment at train time. One of the reasons for better generalization of semantic segmentation and object detection is that these high level abstract representations can be seen as a regularizer which prevents overfitting.

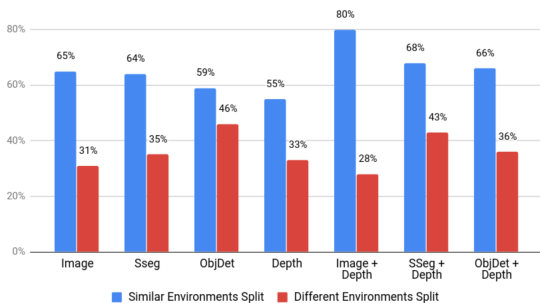


Fig. 4: Comparisons of the performance of different modalities on the splits when the eval environment is similar to the train environment vs when the eval environment is different from the training environment. Only AVD is used for training.

Combination of Feature Extractors: In this section, the effect of combination of feature extractors is evaluated. Unlike the previous section, here the evaluation is done only on the *different environment* split of the AVD dataset to compare generalization of different feature extractors. As it is shown in Fig 5, *ObjDet* and *SSeg* outperform *Depth* with detection being stronger by a margin. Despite segmentation and detection capturing similar information, detection has a larger coverage of general objects, contains all target classes, and is trained on a larger dataset, while segmentation contains more details and only 4 out of the 5 target classes. The results suggest that the former is of higher importance.

Combining the modalities will not always lead to better generalization. Since the real data is limited, it is quite possible to lose generalization with more features. For example, combining all the feature extractors together results in worse performance on the unseen environments compared to using object detector alone. On the other hand, when depth is added to semantic segmentation, the performance improves. Our hypothesis is that if some feature extractors has enough information, combining them will result in overfitting to wrong concepts which leads to poor performance on the unseen environments.

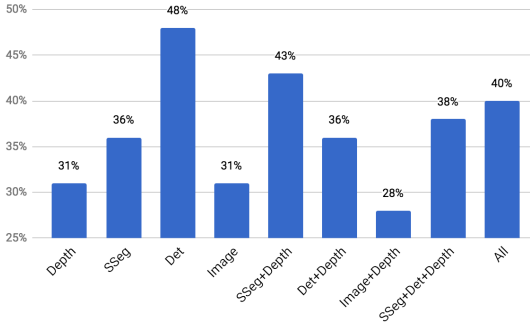


Fig. 5: Comparison of different combination of modalities when trained and tested only on the *different environments* split of AVD.

Knowledge transfer from simulation data to real data: In this section, we evaluate the effect of augmenting training with simulated data from SUNCG dataset. During the training, an episode is sampled uniformly from AVD or SUNCG. The evaluation is done on AVD only.

Results are presented in Fig. 6. We observe that simulated data boosts the performance for *ObjDet* and *SSeg* and their combination. This shows that the proposed representations are capable of using ample simulated data without the need of domain adaptation. The performance increase is in some cases over 10%.

The reality gap, however, is an issue for raw observations, such as *Depth*, where the performance drops. While depth is perfect on SUNCG, on AVD depth is estimated using Kinect, which is noisy and has missing values. We perform data post-processing by capping the max depth at 12m and data augmentation on SUNCG by adding noise to the perfect depth (10% of the points are removed (missing data), and the remaining values have multiplicative noise of 10% added).

Fig. 8 shows the per category accuracy for the *ObjDet* + *SSeg* model. The distribution for the target categories is almost uniform. Out of the three evaluation environments, all the targets are present in two of the environments and in the third environment, target classes `fridge` and `microwave` are present.

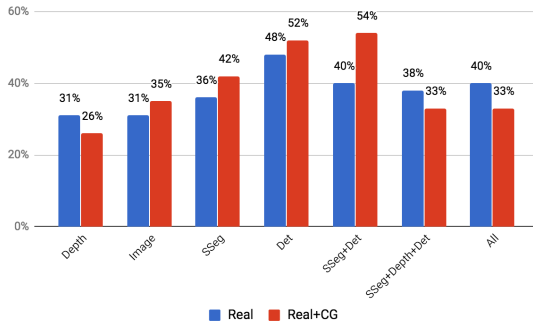


Fig. 6: Effect of simulated data on the success rate (red is training on AVD and SUNCG, while blue is AVD only)

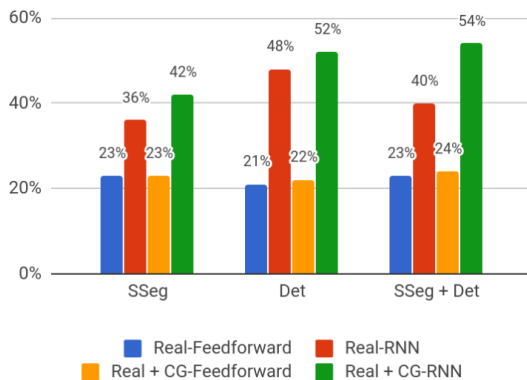


Fig. 7: Effect of ground truth simulation data in helping RNN better model temporal information.

Effect of clean synthetic data on how RNNs capture temporal data:

One possible reason for the performance gain between using only the real data for training versus real data and synthetic CG data is that the RNN actually learns to model the observation better using ground truth detections and segmentations and therefore results in a better performance. To validate this hypothesis we compared the performance of the network on real data and real+synthetic data with or without usage of RNN. As shown in Fig 7 the performance of feed-forward network does not change a lot between the real data and synthetic data but it changes significantly when it is trained with RNN.

4.3 Important Categories for Navigation:

In this section, we quantitatively evaluate what categories are crucial for the model. We choose the model that achieves the best performance on the unseen

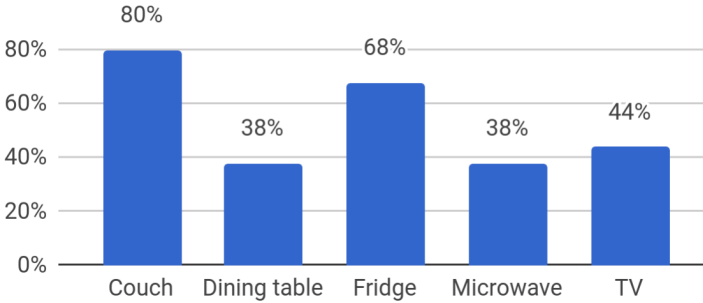


Fig. 8: Per category success rate for $SSeg + ObjDet$.

environments when trained only on real data. In order to evaluate the importance of each category c , the model is trained using all the detection boxes except the ones that have category c . The difference between the performance of the model that uses subset of detections and the model that uses all of the detection boxes, is an indication of how important those categories are for the model. Removing each category of MS-COCO dataset one by one and training a separate model is not feasible due to large number of configurations. Instead, we use the class hierarchy of COCO-stuff dataset [35] to remove the subset of categories that are within the same coarse categories. The coarse categories that we explored are: {Furniture, Kitchen, Appliance, Electronic, Food, Indoor}. Fig 9 shows that the model relies on Furniture coarse category the most. The Furniture contains big objects such as couch, dining table, desk, bed which are visible from far distances and also helps the agent to localizes itself in the houses. On the other hand, coarse category food results in small degradation. Our hypothesis is that these categories are small object which are unlikely to get detected from far distances. Also they provide less semantic context as they can be found in any of the room types.

Comparison with non-learning baseline: In this section, we compare the performance of our method with a traditional method, which assumes that the map of the environment is known. The baseline method has access to the full graph of environment G_e and also the pose for each view in the global coordinate system. The registered poses are provided in the dataset and are computed from 3D reconstruction of all the images for each house.

The baseline agent has two modes. In the first mode, the object detector detects at least one instance of the target category c . In such situation, the location of the object is back-projected to the world coordinate system using the pose of the current view, depth channel, and the intrinsic parameters of the camera. The nearest view from G_e that is directed toward the projected point cloud of the object is chosen as a new destination. Shortest path is computed toward the designated vertex and the agent executes the shortest path without receiving any new observations. If the agent does not see the object, it takes a

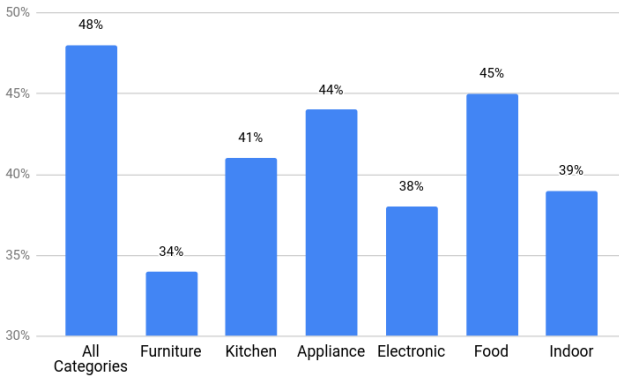


Fig. 9: Effect of removing subset of categories on the success rate of the trained model

random action. Note that even if the object is detected from very far away, the shortest path algorithm on G_e avoids obstacles and computes a path for the part of the scene that is not explored by the agent. Fig 10 illustrates an example of such situation. Note that the accuracy of the baseline methods is affected by the performance of the object detector. The baseline method achieves 46% success rate over the same evaluation set with the same initial poses which shows the strength of our method which can achieve superior performance with significantly more limited knowledge of the environment.

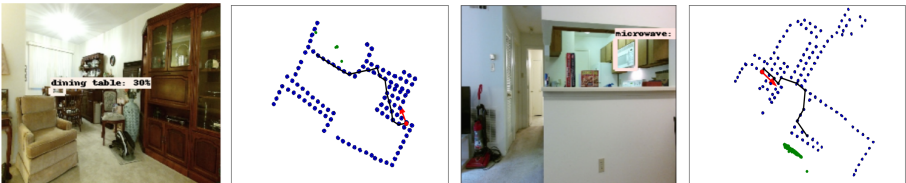


Fig. 10: Illustration of Random+Map baseline uses the map to generate a path toward the object as soon as the agent sees the target object. Red arrow is the robot position, Green is the projected points for the target, and black is the path that is computed from environment graph G_e . For clarity, only detection boxes of the target category is shown.

All the baselines are compared in the table above. In addition to success rate path length ratio metric is also added which is defined only for successful roll outs and it the ratio of the path agent takes over the length of the shortest path from initial point to target views. One of the reasons for the high path length ratio of our method is that action `stop` is not get selected by the policy correctly

Method	Success Rate	Path Length Ratio
Random	14%	58.07
Map + ObjDet	46%	13.88
Our method	54%	29.33

Table 1: Performance comparison of for non-learning baseline and our method

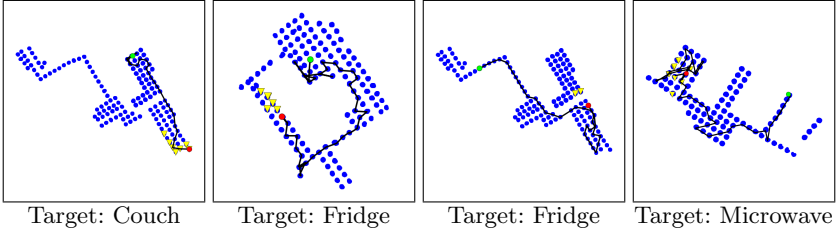


Fig. 11: Visualization of the path generated by the learned policy. Green is the start point, Red is the end point, and yellow triangles represent the target views.

and the agent does not terminate the eval episode properly. When the agent gets close to the goal, it oscillates around the goal and as a result, the path length ratio becomes high. We believe the model does not learn how to properly learn the value of action `stop` because in majority of the situations in training the agent is not close to the target, hence the action `stop` should have small value. Since the distribution for the positive and negative situations is too imbalanced, the model almost always outputs small values for `stop` action which prevents selecting the action.

5 Conclusions

We have demonstrated the use of semantic visual representations obtained from the state-of-the-art detectors and segmentors for target driven visual navigation. These representations were used as observations in training of navigation policy approximated by deep network. The additional appeal of the proposed choice is the ability to train the navigation policies on synthetic CG data jointly with real images without tackling the domain adaptation. The detailed ablations studies of different feature representations demonstrate across the board the effectiveness of semantic segmentation and detectors in generalization to new previously unseen environments. The effect of adding RNN component is most dominant when synthetic data are added to the training. Overall adding training examples from simulated environments improves the generalization capability of the proposed approach, expect when the depth modality is used with both real and synthetic data. The proposed strategy effectively exploits contextual cues learned from visual representations to guide the agent towards the goal 54% of the cases and outperforms the non-learning based baseline which uses the map and state-of-the-art detector by 8%.

References

1. Ammirato, P., Poirson, P., Park, E., Košecka, J., Berg, A.C.: A dataset for developing and benchmarking active vision. In: ICRA. (2017)
2. Cadena, C., Carlone, L., Carrillo, H., Latif, Y., Scaramuzza, D., Neira, J., Reid, I.D., Leonard, J.J.: Simultaneous localization and mapping: Present, future, and the robust-perception age. *IEEE Transactions on Robotics* (2016)
3. Armeni, I., Sener, O., Zamir, A.R., Jiang, H., Brilakis, I., Fischer, M., Savarese, S.: 3D semantic parsing of large-scale indoor spaces. In: CVPR. (2016)
4. Mirowski, P., Pascanu, R., Viola, F., Soyer, H., Ballard, A.J., Banino, A., Denil, M., Goroshin, R., Sifre, L., Kavukcuoglu, K., Kumaran, D., Hadsell, R.: Learning to navigate in complex environments. *ICLR* (2017)
5. Oh, J., Chockalingam, V., Singh, S., Lee, H.: Control of memory, active perception, and action in Minecraft. *ArXiv arXiv:1605.09128* (2001)
6. Bruce, J., Sünderhauf, N., Mirowski, P., Hadsell, R., Milford, M.: One-shot reinforcement learning for robot navigation with interactive replay. *ArXiv arXiv:1711.10137* (2017)
7. Zhu, Y., Mottaghi, R., Kolve, E., Lim, J.J., Gupta, A., Fei-Fei, L., Farhadi, A.: Target-driven visual navigation in indoor scenes using deep reinforcement learning. *CVPR* (2017)
8. Wu, Y., Wu, Y., Gkioxari, G., Tian, Y.: Building generalizable agents with a realistic and rich 3D environment. In: NIPS Deep Reinforcement Learning Symposium. (2017)
9. Hochreiter, S., Schmidhuber, J.: Long short-term memory. *Neural computation* **9**(8) (1997) 1735–1780
10. Song, S., Yu, F., Zeng, A., Chang, A.X., Savva, M., Funkhouser, T.: Semantic scene completion from a single depth image. *CVPR* (2017)
11. Faust, A., Ramirez, O., Fiser, M., Oslund, K., Francis, A., Davidson, J., Tapia, L.: PRM-RL: long-range robotic navigation tasks by combining reinforcement learning and sampling-based planning. In: ICRA. (2018)
12. Gupta, S., Davidson, J., Levine, S., Sukthankar, R., Malik, J.: Cognitive mapping and planning for visual navigation. *CVPR* (2017)
13. Mnih, V., Badia, A.P., Mirza, M., Graves, A., Lillicrap, T.P., Harley, T., Silver, D., Kavukcuoglu, K.: Asynchronous methods for deep reinforcement learning. *ICML* (2016)
14. Mirowski, P., Pascanu, R., Viola, F., Soyer, H., Ballard, A.J., Banino, A., Denil, M., Goroshin, R., Sifre, L., Kavukcuoglu, K., Kumaran, D., Hadsell, R.: Learning to navigate in complex environments. *ArXiv arXiv:1611.03673* (2017)
15. Dosovitskiy, A., Koltun, V.: Learning to act by predicting future. *ICLR* (2017)
16. Savva, M., Chang, A.X., Dosovitskiy, A., Funkhouser, T., Koltun, V.: Minos: Multimodal indoor simulator for navigation in complex environments simulated environment for studying goal directed navigation. *ArXiv:1712.03931* (2017)
17. Chang, A., Dai, A., Funkhouser, T., Halber, M., Niessner, M., Savva, M., Song, S., Zeng, A., Zhang, Y.: Matterport3d: Learning from RGB-D data in indoor environments. *3DV* (2017)
18. Zamir, A., Xia, F., He, Z.Y., Sax, S.: Gibson environment for embodied real-world active perception. *CVPR (to appear)* (2018)
19. Gordon, D., Kembhavi, A., Rastegari, M., Redmon, J., Fox, D., Farhadi, A.: IQA: Visual question answering in interactive environments. *ArXiv:1712.03316* (2017)

20. Das, A., Datta, S., Gkioxari, G., Lee, S., Parikh, D., Batra, D.: Embodied question answering. *CVPR (to appear)* (2018)
21. Khan, A., Zhang, C., Atanasov, N., Karydis, K., Kumar, V., Lee, D.D.: Memory augmented control networks. *ArXiv arXiv:1709.05706* (2017)
22. Szegedy, C., Ioffe, S., Vanhoucke, V., Alemi, A.A.: Inception-v4, inception-resnet and the impact of residual connections on learning. In: *AAAI*. Volume 4. (2017) 12
23. He, K., Zhang, X., Ren, S., Sun, J.: Deep residual learning for image recognition. In: *CVPR*. (2016) 770–778
24. Deng, J., Dong, W., Socher, R., Li, L.J., Li, K., Fei-Fei, L.: ImageNet: A large-scale hierarchical image database. In: *CVPR, IEEE* (2009) 248–255
25. Ren, S., He, K., Girshick, R., Sun, J.: Faster r-cnn: Towards real-time object detection with region proposal networks. In: *Advances in neural information processing systems*. (2015) 91–99
26. Lin, T.Y., Maire, M., Belongie, S., Hays, J., Perona, P., Ramanan, D., Dollr, P., Zitnick, C.L.: Microsoft COCO: Common objects in context. In: *ECCV*. (2014)
27. Mousavian, A., Pirsiavash, H., Košečka, J.: Joint semantic segmentation and depth estimation with deep convolutional networks. *3DV* (2016)
28. Silberman, N., Hoiem, D., Kohli, P., Fergus, R.: Indoor segmentation and support inference from rgb-d images. *ECCV* (2012)
29. Ganin, Y., Lempitsky, V.: Unsupervised domain adaptation by backpropagation. In: *ICML*. (2015) 1180–1189
30. Bousmalis, K., Silberman, N., Dohan, D., Erhan, D., Krishnan, D.: Unsupervised pixel-level domain adaptation with generative adversarial networks. In: *CVPR*. (2017)
31. Bousmalis, K., Irpan, A., Wohlhart, P., Bai, Y., Kelcey, M., Kalakrishnan, M., Downs, L., Ibarz, J., Pastor, P., Konolige, K., Levine, S., Vanhoucke, V.: Using simulation and domain adaptation to improve efficiency of deep robotic grasping. *ICRA (to appear)* (2018)
32. Chen, L., Papandreou, G., Kokkinos, I., Murphy, K., Yuille, A.L.: Deeplab: Semantic image segmentation with deep convolutional nets, atrous convolution, and fully connected CRFs. *CVPR* (2016)
33. Argall, B.D., Chernova, S., Veloso, M., Browning, B.: A survey of robot learning from demonstration. *Robotics and autonomous systems* **57**(5) (2009) 469–483
34. Ross, S., Gordon, G., Bagnell, D.: A reduction of imitation learning and structured prediction to no-regret online learning. In: *AISTATS*. (2011) 627–635
35. Caesar, H., Uijlings, J., Ferrari, V.: Coco-stuff: Thing and stuff classes in context. In: *Computer vision and pattern recognition (CVPR), 2018 IEEE conference on, IEEE* (2018)